ISSN 1027-4510, Journal of Surface Investigation: X-ray, Synchrotron and Neutron Techniques, 2023, Vol. 17, No. 6, pp. 1514–1519. © Pleiades Publishing, Ltd., 2023.

Features of the Conduction-Band Electronic Structure of Manganese Sulfide Solid Solutions Doped with Lanthanides

M. M. Syrokvashin[a, *], E. V. Korotaev[a], A. D. Nikolenko[b, c], and V. V. Kriventsov[d]

[a] *Nikolaev Institute of Inorganic Chemistry, Siberian Branch, Russian Academy of Sciences, Novosibirsk, 630090 Russia*

[b] *Budker Institute of Nuclear Physics, Siberian Branch, Russian Academy of Sciences, Novosibirsk, 630090 Russia*

[c] *Center for Collective Use "Siberian Ring Photon Source" (SKIF), Boreskov Institute of Catalysis, Siberian Branch, Russian Academy of Sciences, Koltsovo, 630559 Russia*

[d] *Boreskov Institute of Catalysis, Siberian Branch, Russian Academy of Sciences, Novosibirsk, 630090 Russia*

**e-mail: syrokvashin@niic.nsc.ru*

Received April 7, 2023; revised June 24, 2023; accepted June 24, 2023

Abstract—Studying the X-ray absorption near-edge structure shows that cation substitution of a MnS matrix with lanthanide atoms does not significantly affect the character of the local environment of metal (manganese, dysprosium, thulium and ytterbium) and sulfur atoms in lanthanide-doped $Ln_{0.05}Mn_{0.95}S$ (*Ln* = Dy, Tm, Yb) solid solutions. Comparison of the experimental and theoretical data obtained by the finite-difference method has revealed that the main contributions of the unoccupied *p*- and *d*-states of manganese and *p*-states of sulfur are localized at the conduction-band bottom, both in the case of the initial MnS matrix and in the case of lanthanide-substituted $Ln_{0.05}Mn_{0.95}S$ solid solutions. The main contributions of unoccupied *f*-states of ytterbium and thulium in $Ln_{0.05}Mn_{0.95}S$ (*Ln* = Tm, Yb) solid solutions are shifted to the high-energy region of the conduction band, while the *f*-states of dysprosium in dysprosium-doped $Dy_{0.05}Mn_{0.95}S$ solid solutions are localized near the conduction-band bottom. According to the calculated model spectra, it is found that the contributions of the free lanthanide *d*-states in $Ln_{0.05}Mn_{0.95}S$ (*Ln* = Dy, Tm, Yb) solid solutions are shifted to the region of the conduction-band bottom with an increase of the atomic number of the lanthanide atom.

Keywords: manganese sulfide, lanthanides, finite-difference method, density of states, X-ray absorption near-edge structure, density-functional theory

DOI: 10.1134/S1027451023060460

INTRODUCTION

Currently, one of the areas of materials science under development is the search for highly efficient thermoelectric materials based on sulfides of transition and rare-earth metals [1–6]. One of the representatives of this class of compounds are cation-substituted manganese sulfides $M_xMn_{1-x}S$(*M* is a transition or rare-earth metal), for which there is data on high values of the Seebeck coefficient ($S \sim -8000\ldots 900$ μV/K [7–10]; $S \sim 18000$ μV/K [11]). The physical properties of solid solutions can be controlled by changing the type and concentration of substituting atoms. However, an increase in the degree of cation substitution in $M_xMn_{1-x}S$ above $x > 0.05$ leads to the appearance of a metal–dielectric concentration transition, which results in a change in the electrical properties due to rearrangement of the electronic structure in the process of cation substitution [5–7, 12, 13]. The electrophysical properties of thermoelectric materials largely depend on the features of the structure of the electronic structure. The Seebeck coefficient of semiconductors *S* can be calculated by the following formula [2, 5]:

$$S = -\frac{k}{e}\left(\frac{\left(\ln\frac{N_c}{n}+2\right)n\mu_n - \left(\ln\frac{N_v}{p}+2\right)p\mu_p}{n\mu_n + p\mu_p}\right), \quad (1)$$

where *k* is the Boltzmann constant; *e* is the elementary charge; N_c and N_v are the effective density of states in the conduction and valence bands, respectively; *n*, *p*, μ_n, and μ_p are the concentration and mobility of electrons (*n*) and holes (*p*) respectively. As can be seen from expression (1), in addition to the components associated with the concentration and characteristics of charge carriers, the Seebeck coefficient of semiconductors is determined by the distribution of the density of states in the conduction and valence bands. Thus, one can conclude that understanding the features of the formation of an electronic structure is one of the key aspects in optimizing, predicting, and interpreting the thermoelectric properties of functional materials.

The corresponding information can be obtained using both experimental methods of spectroscopy and theoretical methods of quantum chemistry. The purpose of this work is to conduct a comprehensive study of the features of the formation of the conduction band of the initial MnS matrix and $Ln_xMn_{1-x}S$ solid solutions on its basis by analyzing the structure of the X-ray absorption near-edge structure (XANES) and comparing experimental data with the results of modeling the density of free states.

EXPERIMENTAL

Powder samples $Ln_xMn_{1-x}S$(Ln = Dy, Tm, Yb; x = 0; 0.05) were obtained by solid-phase synthesis from industrial metal oxides in a sulfiding atmosphere. Manganese oxide MnO_2 was used as the initial solid reagents (Technical Specification (TU) 6-09-5198-84) and rare-earth metals Dy_2O_3, Tm_2O_3 and Yb_2O_3 (brands DiO-I, TuO-I and IbO-V) with a purity of 99.99%. A mixture of oxides in the required stoichiometric ratio was thoroughly ground in an agate mortar for ~30 min. Next, the resulting mixture was placed in a glassy carbon boat that was loaded into a horizontal quartz reactor, in which the required temperature was set to ~1050°C. The thermolysis products of ammonium thiocyanate NH_4CNS (State Standard (GOST 27067–86)) were used as the sulfiding reagent [14]. The control of the completeness of sulfidation was carried out by weighing and X-ray phase analysis [15, 16].

The X-ray absorption spectra of lanthanides Ln = Dy, Tm, Yb (L_3 edge) and manganese (K edge) were obtained in the transmission mode using synchrotron radiation at the VEPP-3 storage ring at the EXAFS spectroscopy station of the Center for Collective Use of the Siberian Center for Synchrotron and Terahertz Radiation (Budker Institute of Nuclear Physics, Siberian Branch, Russian Academy of Sciences, Novosibirsk). We used a two-crystal Si(111) monochromator with an energy resolution ($\Delta E/E$) of 1.6×10^{-4} in the studied energy range. For each sample, weights were made for the optimal absorption jump. To obtain the spectra, the test compounds were ground and pressed with cellulose, transparent in the studied X-ray range.

The X-ray absorption spectra of sulfur (K edge) were obtained in the transmission mode using synchrotron radiation at the VEPP-4 storage ring on the Kosmos metrological station at the Center for Collective Use of the Siberian Center for Synchrotron and Terahertz Radiation (Budker Institute of Nuclear Physics, Siberian Branch, Russian Academy of Sciences, Novosibirsk). The experiments were carried out using a two-crystal Si(111) monochromator with an energy resolution of $\Delta E/E = 1 \times 10^{-4}$ in the studied energy range. To obtain spectra using glue, the samples were uniformly applied to a Mylar film 3 μm thick. Each absorber consisted of two film layers with a deposited sample.

Simulation of the XANES spectra and calculation of the partial densities of states were carried out by the finite-difference method in the FDMNES software package [17, 18]. The Hedin–Lanqvist potential was used as the exchange-correlation potential. To simulate the XANES spectra of $Ln_xMn_{1-x}S$ solid solutions of one and four nonequivalent manganese atoms has been replaced by a lanthanide atom (Dy, Tm or Yb), we used the values obtained on the basis of the X-ray phase analysis data as the lattice parameter a. Inside the cluster under consideration, the potential created by atoms was described in terms of the local electron density approximation. In the course of the calculations, the optimal cluster size of 8.5 Å (out of 147 atoms) was selected, which ensures the best agreement between the theoretical and experimental spectra.

RESULTS AND DISCUSSION

The X-ray absorption K edge of sulfur for powder samples of the initial MnS matrix and $Ln_{0.05}Mn_{0.95}S$ (Ln = Dy, Tm, Yb) solid solutions are shown in Fig. 1. A comparison of the structure of the absorption spectra of MnS showed that the main features of the experimental XANES spectra (features A–G in Fig. 1) are retained for all studied compositions. The similarity of the structure of the spectra of cation-substituted solid solutions and the initial matrix allows us to conclude that in $Ln_{0.05}Mn_{0.95}S$, the structural type of the initial matrix is retained, and the nature of the local environment of sulfur atoms does not change. It can also be noted that the energy position and structure of the absorption spectrum sulfur K edge for the MnS matrix agrees well with the data obtained in [19–21]. The obsence of the changes in the pre-edge structure (features A and B in Fig. 1) of the absorption edge of the solid solutions indicates that cation substitution does not significantly affect the nature of the local environment of sulfur atoms.

To study the features of the formation of the conduction band, modeling of the experimental XANES spectra $Ln_xMn_{1-x}S$ was carried out (marked "Calculation" in Fig. 1). It should be noted that, in this case, the model absorption spectra are presented without taking into account the instrumental broadening and the width of the internal level from which an electron was knocked out. For convenience of comparison with experimental data, the model spectra and partial contributions of the densities of states are presented on an arbitrary scale, and the ratio of the partial contributions to each other is retained and corresponds to the output data of the FDMNES software package. Comparison of the structure of the experimental absorption sulfur K edges (denoted "Experiment") with the results of calculations showed that the main contribution to the structure of the spectrum near the absorption edge is made by the density of p-states of sulfur (features A–G) and free p-states of atoms corresponding to $1s \rightarrow np$ dipole transitions. In the pre-edge (fea-

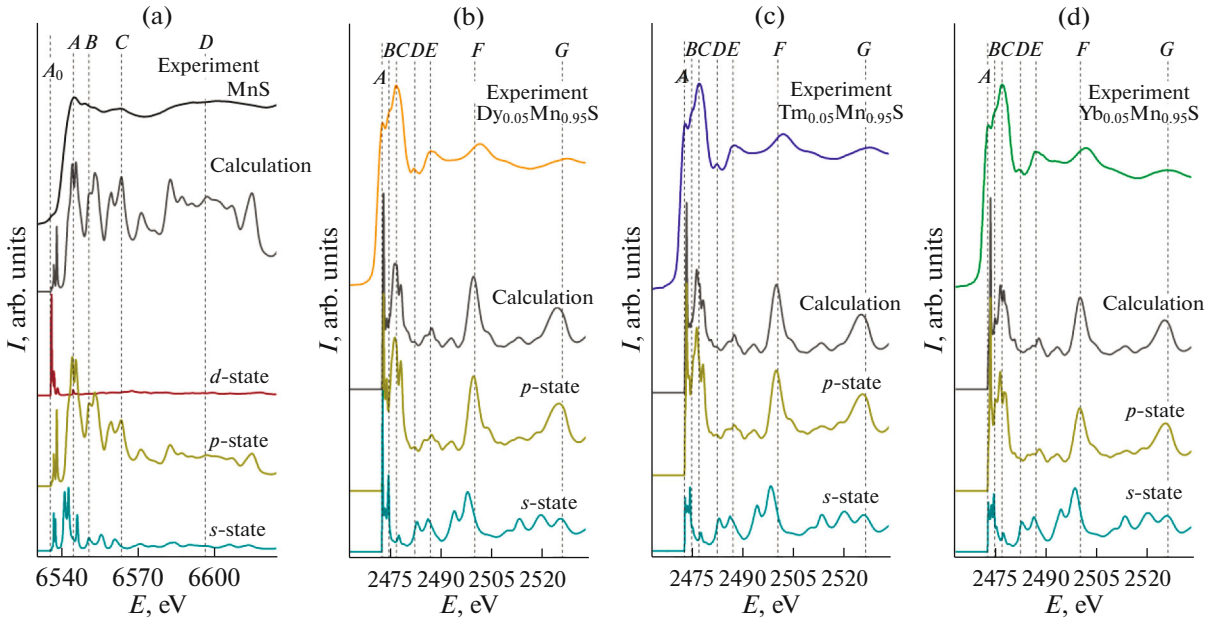

Fig. 1. Experimental and calculated *K* edges and the partial contributions of *p*- and *s*-states of sulfur for the initial MnS matrix (a) and lanthanide-substituted solid solutions $Ln_{0.05}Mn_{0.95}S$ (*Ln* = Dy (b), Tm (c), and Yb (d)).

ture *A*) and high-energy region of the experimental spectra (features *E* and *F*) there are maxima that correspond to the maxima of the *s*- and *p*-states of sulfur. However, according to selection rules, the transitions $1s \rightarrow ns$ are forbidden and probably a correlation between the structure of *s*-states and the corresponding spectral features due to the hybridization of *s*- and *p*-states in the region of lower free states of the conduction band due to chemical bonding.

In the case of the *K* absorption edge of manganese, comparison of the experimental data ("Experiment" in Fig. 2) and the results of modeling partial contributions of the density of states (denoted "Calculation") showed that the main contribution to the structure of the edge (features *A*–*C*) is brought by free *p* states of manganese atoms. The presence of the pre-edge feature A_0 is due to contributions of the *p*- and *d* states of manganese atoms. The contribution of *d*-states into the structure of the corresponding absorption maximum is due to the hybridization of *p*- and *d*-states, as well as the presence of a significant electron density on the *d*-shell of Mn^2 [22]. The absorption maximum in the experimental *K* edges corresponding to *s*-states of manganese atoms is localized near the features *A* and *B*. However, since, according to selection rules, transitions $1s \rightarrow ns$ are prohibited, as in the case of the *K* absorption edge of sulfur, correlation between the structure of the *s*-states and the corresponding spectral features is due to the appearance of the hybridization of free *s*- and *p*-states of manganese atoms. The structure of the high-energy feature *D* is mainly a result of the contributions of *p*-states of manganese atoms, which is due to the fact that the probability of $1s \rightarrow np$ dipole transitions is larger in comparison with that for $1s \rightarrow nd$ quadrupole transitions. Thus, we can conclude that the structure of the spectral feature *D* is mainly due to the contributions of free *p*-states.

Analysis of partial contributions of the free states electron density the L_3 absorption edge of lanthanides (Fig. 3) showed that the largest contribution to the structure of the main maximum of the L_3 edge (features *A* and *B*) is made by the *s*- and *d*-states of the lanthanides. This is due to the fact that the probability of $2p \rightarrow ns$ and $2p \rightarrow nd$ dipole transitions is greater than in the case of $2p \rightarrow nf$ quadrupole transitions, and $2p \rightarrow np$ transitions are prohibited. In the case of $Dy_{0.05}Mn_{0.95}S$, the calculated spectrum near the L_3 edge of dysprosium has a similar structure with the spectra near the L_3 edge of thulium and ytterbium in $Ln_{0.05}Mn_{0.95}S$ (*Ln* = Tm, Yb). The structure of the main maximum of the absorption edge (features *A* and *B*) is also due to the contributions of the *s*- and *d*-states of lanthanide atoms. However, for the L_3 edge of dysprosium, in contrast to thulium and ytterbium, the main contribution of *f*-states is localized in the low-energy region of the bottom of the conduction band, which is probably due to partial filling of the *f*-shell of dysprosium, which is less than in the case of thulium and ytterbium atoms.

Representation of the experimental (Fig. 4a) and model (Figs. 4b and 4c) XANES spectra of metals and sulfur on a single energy scale makes it possible to determine the nature of the distribution of free states in the conduction band. For greater clarity, Fig. 4 shows the model spectra both with instrumental

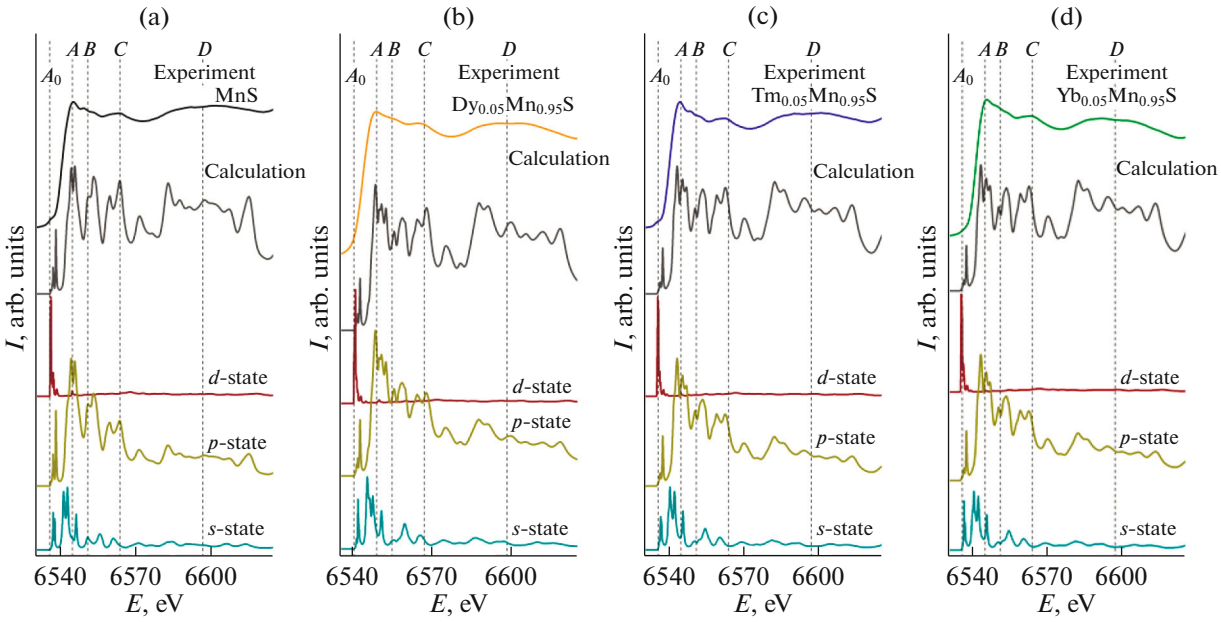

Fig. 2. Experimental and calculated *K* edges and partial contributions of *d*-, *p*-, and *s*-states of manganese for the initial MnS matrix (a) and lanthanide-substituted solid solutions $Ln_{0.05}Mn_{0.95}S$ (*Ln* = Dy (b), Tm (c), and Yb (d)).

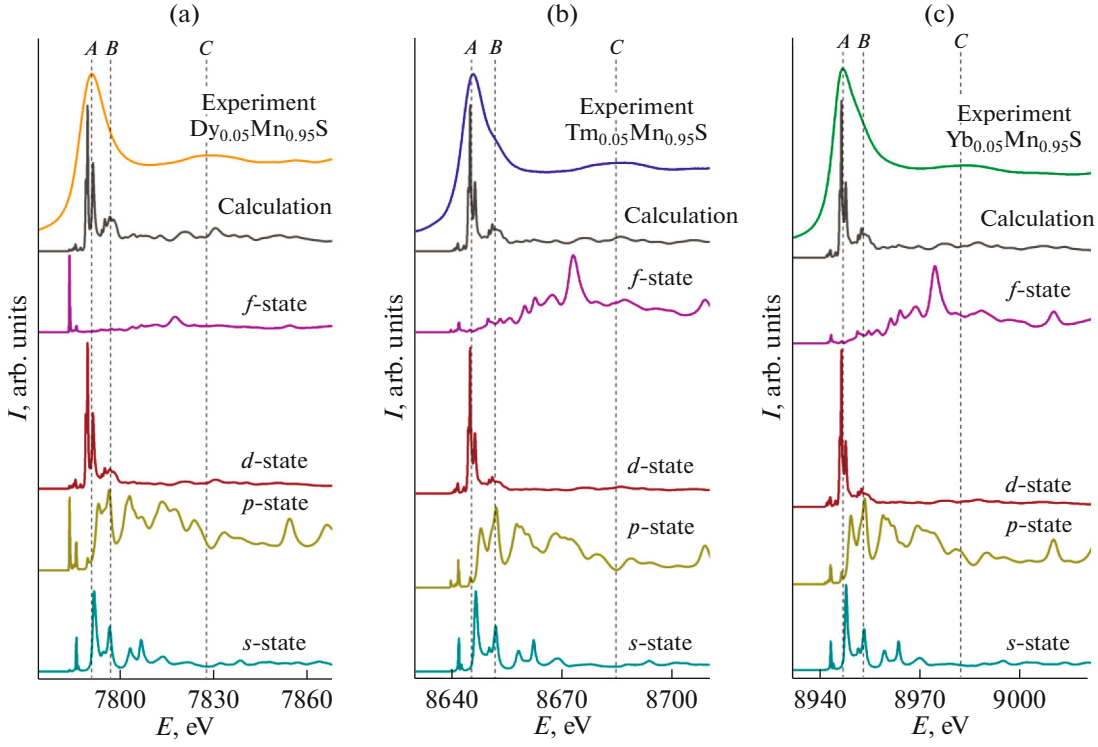

Fig. 3. Experimental and calculated L_3 edges and partial contributions *f*-, *d*-, *p*-, and *s*-states of lanthanides for solid solutions $Ln_{0.05}Mn_{0.95}S$ (Ln = Dy (a), Tm (b), and Yb (c)).

broadening (Fig. 4b) and without it (Fig. 4c). The lower free states in the conduction band in $Ln_xMn_{1-x}S$ correspond to the *np*-states of sulfur (Fig. 1) and the *nd*-states of manganese (Fig. 2). Cation substitution of the initial MnS matrix leads to the appearance of contributions of the *nd*-states of lanthanides in the energy

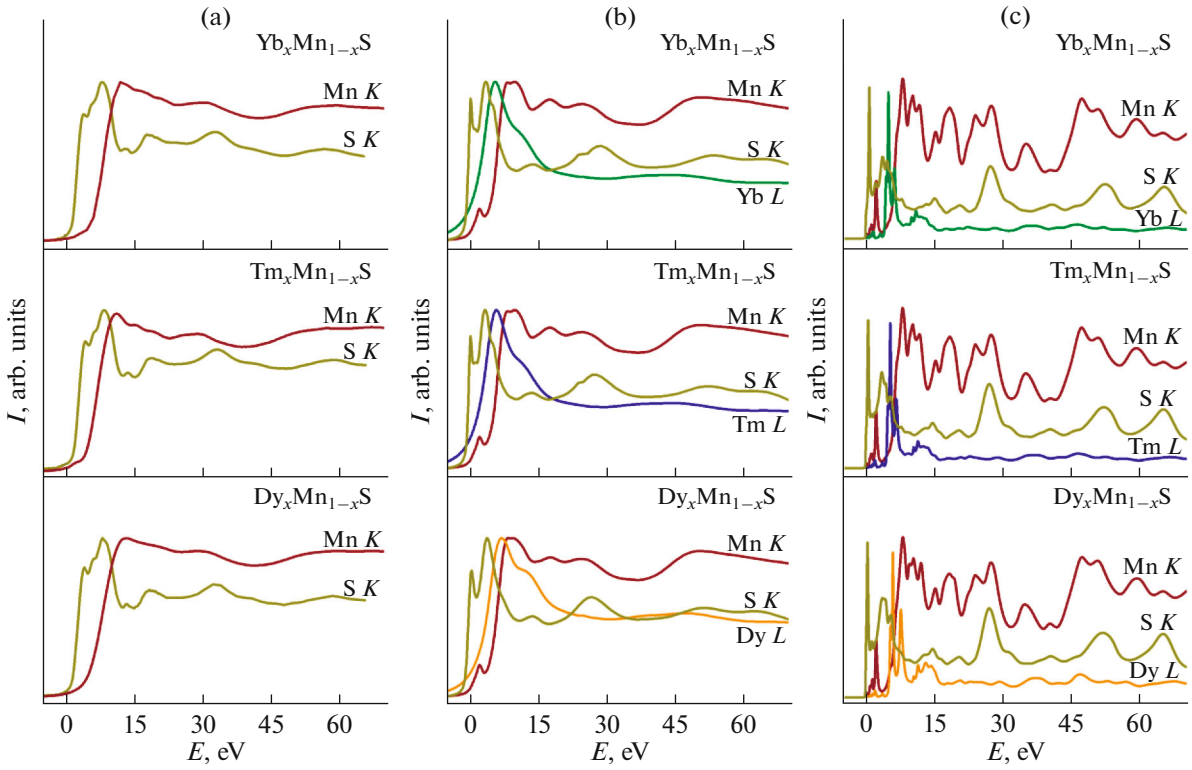

Fig. 4. Representation of XANES spectra $Ln_xMn_{1-x}S$(Ln = Dy, Tm, Yb) on a unified energy scale: experimental data (a), and model spectra with (b) and without instrumental broadening (c).

structure of the bottom of the conduction band (Fig. 3). It can also be noted that the corresponding contribution shifts to the bottom of the conduction band with an increase in the atomic number of the lanthanide atom (Figs. 4b and 4c). An analysis of the partial contributions of the states to the absorption spectra showed that in the case of solid solutions with dysprosium $Dy_xMn_{1-x}S$ in the region of the bottom of the conduction band, there is also a significant contribution of *nf*-states of dysprosium atoms (Fig. 3). In the high-energy region of the conduction band, there are contributions of *np*- and *nd*-states of manganese, *np*-states of sulfur, as well as *nf*-states of the lanthanides. Thus, the energy binding of the experimental spectra of metals and sulfur confirms the mutual arrangement of the contributions of the corresponding elements in the structure of the conduction band.

CONCLUSIONS

A joint study of the fine structure of the XANES spectra and data on the distribution of the density of states obtained by quantum-chemistry methods made it possible to obtain data on the features of the electronic structure of the conduction band of the initial MnS matrix and lanthanide-substituted solid solutions $Ln_{0.05}Mn_{0.95}S$ (Ln = Dy, Tm, Yb). It is shown that the main contributions of free *p*- and *d*-states of manganese and *p*-states of sulfur are localized in the region of the bottom of the conduction band. Major contributions of free *f*-states of ytterbium and thulium are shifted in the high-energy region relative to the bottom of the conduction band, while the *f*-states of dysprosium are localized in the bottom of the conduction band. The contributions of free *d*-states of lanthanides shifts to the bottom of the conduction band with an increase in the atomic number of the lanthanide atom.

FUNDING

M.M. Syrokvashin and E.V. Korotaev are grateful to the Ministry of Science and Higher Education of the Russian Federation (project no. 121031700313-8). To obtain experimental data the equipment of the Center for Collective Use "Siberian Ring Photon Source" (SKIF) (on the basis of the Unique Scientific Installation "Complex VEPP-4–VEPP-2000" at the Budker Institute of Nuclear Physics, Siberian Branch, Russian Academy of Sciences, was used. V.V. Kriventsov expresses his gratitude to the Ministry for Science and Higher Education of the Russian Federation for financial support within the framework of the state task for the Boreskov Institute of Catalysis, Siberian Branch, Russian Academy of Sciences.

CONFLICT OF INTEREST

The authors declare that they have no conflicts of interest.

REFERENCES

1. A. V. Sotnikov, M. M. Syrokvashin, V. V. Bakovets, I. Yu. Filatova, E. V. Korotaev, A. Sh. Agazhanov, and D. A. Samoshkin, J. Am. Ceram. Soc. **105**, 2813 (2022). https://www.doi.org/10.1111/jace.18292
2. E. V. Korotaev, M. M. Syrokvashin, I. Y. Filatova, A. V. Kalinkin, and A. V. Sotnikov, Sci. Rep. **11**, 18934 (2021). https://www.doi.org/10.1038/s41598-021-98350-9
3. A. V. Sotnikov, P. Jood, and M. Ohta, ACS Omega **5**, 13006 (2020). https://www.doi.org/10.1021/acsomega.0c00908
4. V. V. Sokolov, V. V. Bakovetz, S. M. Luguev, and N. V. Lugueva, Adv. Mater. Phys. Chem. **2**, 25 (2012). https://www.doi.org/10.4236/ampc.2012.24B007
5. E. V. Korotaev, M. M. Syrokvashin, I. Y. Filatova, K. G. Pelmenev, V. V. Zvereva, N. N. Peregudova, J. Electron. Mater. **47**, 33923397 (2018). https://www.doi.org/10.1007/s11664-018-6230-9
6. S. S. Aplesnin, O. B. Romanova, A. M. Khar'kov, and A. I. Galyas, Phys. Solid State **58**, 19 (2016). https://www.doi.org/10.1134/S1063783416010029
7. O. B. Romanova, L. I. Ryabinkina, V. V. Sokolov, A. Y. Pichugin, D. A. Velikanov, D. A. Balaev, A. I. Galyas, O. F. Demidenko, G. I. Makovetskii, and K. I. Yanushkevich, Solid State Commun. **150**, 602 (2010). https://www.doi.org/10.1016/j.ssc.2009.12.042
8. G. I. Makovetskii, A. I. Galyas, O. F. Demidenko, K. I. Yanushkevich, L. I. Ryabinkina, and O. B. Romanova, Phys. Solid State **50**, 1826 (2008). https://www.doi.org/10.1134/S1063783408100065
9. O. B. Romanova, S. S. Aplesnin, A. M. Khar'kov, V. V. Kretinin, and A. M. Zhivul'ko, Phys. Solid State **60**, 1691 (2018). https://www.doi.org/10.1134/S1063783418090263
10. S. S. Aplesnin, O. B. Romanova, A. I. Galyas, and V. V. Sokolov, Phys. Solid State **57**, 886 (2015). https://www.doi.org/10.1134/S1063783415050029
11. S. S. Aplesnin and M. N. Sitnikov, JETP Lett. **100**, 95 (2014). https://www.doi.org/10.1134/S0021364014140021
12. S. Aplesnin, O. Romanova, A. Har'kov, D. Balaev, M. Gorev, A. Vorotinov, V. Sokolov, and A. Pichugin, Phys. Status Solidi B **249**, 812 (2012). https://www.doi.org/10.1002/pssb.201147327
13. E. V. Korotaev, M. M. Syrokvashin, I. Y. Filatova, S. V. Trubina, A. D. Nikolenko, D. V. Ivlyushkin, P. S. Zavertkin, A. V. Sotnikov, and V. V. Kriventsov, Appl. Phys. A **126**, 537 (2020). https://www.doi.org/10.1007/s00339-020-03715-y
14. A. V. Sotnikov, V. V. Bakovets, V. V. Sokolov, and I. Yu. Filatova, Inorg. Mater. **50**, 10241029 (2014). https://www.doi.org/10.1134/S0020168514100173
15. M. M. Syrokvashin, E. V. Korotaev, N. A. Kryuchkova, V. V. Zvereva, I. Y. Filatova, and A. V. Kalinkin, Appl. Surf. Sci. **492**, 209218 (2019). https://www.doi.org/10.1016/j.apsusc.2019.05.237
16. M. M. Syrokvashin, E. V. Korotaev, I. Y. Filatova, S. V. Trubina, and S. B. Erenburg, Spectrochim. Acta, Part A **205**, 593 (2018). https://www.doi.org/10.1016/j.saa.2018.07.053
17. S. A. Guda, A. A. Guda, M. A. Soldatov, K. A. Lomachenko, A. L. Bugaev, C. Lamberti, W. Gawelda, C. Bressler, G. Smolentsev, A. V. Soldatov, and Y. Joly, J. Chem. Theory Comput. **11**, 4512 (2015). https://doi.org/10.1021/acs.jctc.5b00327
18. Y. Joly, Phys. Rev. B **63**, 125120 (2001). https://doi.org/10.1103/PhysRevB.63.125120
19. S. P. Farrell, M. E. Fleet, I. E. Stekhin, A. Kravtsova, A. V. Soldatov, and X. Liu, Am. Mineral. **87**, 1321 (2002). https://www.doi.org/10.2138/am-2002-1007
20. K. A. Evans, H. S. C. O' Neill, J. A. Mavrogenes, N. S. Keller, L.-Y. Jang, and J.-F. Lee, Geochim. Cosmochim. Acta **73**, 6847 (2009). https://www.doi.org/10.1016/j.gca.2009.08.013
21. K. Kim, S. Asaoka, T. Yamamoto, S. Hayakawa, K. Takeda, M. Katayama, and T. Onoue, Environ. Sci. Technol. **46**, 10169 (2012). https://www.doi.org/10.1021/es301575u
22. E. V. Korotaev, M. M. Syrokvashin, I. Yu. Filatova, S. V. Trubina, A. D. Nikolenko, D. V. Ivlyushkin, P. S. Zavertkin, and V. V. Kriventsov, AIP Conf. Proc. **2299**, 080004 (2020). https://www.doi.org/10.1063/5.0030414